

Multiscale Ultrabroadband Polymer Scattering Media with Tailored Emittance for Radiative Thermal Management

Zhenpeng Li¹, Mathis Degeorges¹, Nithin Jo Varghese¹, Jyotirmoy Mandal^{1,2*}

¹Department of Civil and Environmental Engineering, Princeton University, Princeton, USA

²Princeton Materials Institute, Princeton University, Princeton, USA

*Corresponding author: Jyotirmoy Mandal (jm3136@princeton.edu)

Abstract

A surface that selectively emits heat in the long-wave infrared (LWIR) can enable passive cooling in hot environments while retaining partial radiative insulation in cold conditions, but its real-world deployment is limited by reliance on ultrabroadband metallic reflectors such as silver. Here we engineer random photonic media with a layered, multiscale scattering architecture to simultaneously achieve ultraviolet-to-far-infrared reflection and selective LWIR emission. We validate our approach by developing a metal-free selective emitter that exhibits high LWIR emittance (0.88), strong solar reflectance (0.97), and low thermal emittance outside the LWIR (0.49), independent of the substrate. Field tests, supported by theoretical modeling, show enhanced radiative cooling and thermoregulation across diverse applications relative to conventional broadband emitters. Leveraging the low cost and scalable manufacturing of scattering media, this work provides a pathway to advance radiative thermal management, enabling energy saving and improved thermal comfort.

Introduction

Spectrally selective control of light is critical to many fields like thermal photonics, energy harvesting, and imaging, but also presents perennial challenge due to its requirement of sophisticated structural and material engineering at multiple scales.¹⁻⁴ A notable example is radiative thermoregulation, which requires spectral control of both solar ($\lambda \sim 0.3\text{-}2.5 \mu\text{m}$) and thermal infrared (TIR, $\lambda \sim 2.5\text{-}30 \mu\text{m}$) light at scales and costs practical for use. In recent years, this has been extensively studied for passive radiative cooling, which ideally requires materials with ultrabroadband reflectance at $\lambda \sim 0.3\text{-}8 \mu\text{m}$ and $\sim 13\text{-}30 \mu\text{m}$, and a selective wideband emittance in the longwave infrared (LWIR, $\lambda \sim 8\text{-}13 \mu\text{m}$) waveband (Fig. S1).⁵ Such radiative coolers (RCs) are radiatively shielded from the sun and quasi-isolated from both atmospheric and terrestrial radiation, but can still access the heat sink of space through the atmosphere's LWIR transmission window. Deployed at envelopes' surfaces, they can passively regulate heat flows to benefit buildings, devices, human bodies, and potentially, broader environment.

However, achieving wideband optical selectivity over the ultrabroad solar-to-TIR waveband, which spans two orders of magnitude in wavelength ($0.3\text{-}30 \mu\text{m}$), is challenging. This arises from multiple factors, including intrinsically broadband optical properties of materials (e.g., the broadband TIR emittances of most dielectrics like ceramics and polymers),⁶ and morphologies that are necessary for desired optical properties (e.g., optical thickness required for high LWIR emittance), but lend to broadband behavior. Indeed, most RCs are broadband thermal emitters.⁷⁻⁹ For sky-facing designs, this may limit cooling performances, and on exterior facades, cause undesirable terrestrial heat gains or losses.¹⁰ Of the selective LWIR emitters that exist, the overwhelming majority employ the architecture where a LWIR-emissive material with controlled thickness is placed over an ultrabroadband metal reflector, usually silver (Tables S1-S2).^{5,10-13} The handful of exceptions employ bulk ceramics with suitable Reststrahlen reflectance bands to achieve selective emittance.^{10,14,15} Both these architectures have been long-known,¹⁶ but face limitations. For instance, the corrodibility, specular glare, impermeability, and intrinsic limits on the solar reflectance of metal films could hinder their practical performance and widespread deployment.¹⁷⁻¹⁹ Reported Reststrahlen reflective ceramics are less practical still, as they are costly to fabricate at scale and are susceptible to weathering.^{20,21}

Beyond relying on free electrons in metals or optical phonons in polar crystals to reflect light, another promising optical paradigm is to exploit random media comprising polydisperse lossless scatterers, which enable multiple scattering and thus high reflection of broadband light.²²⁻²⁴ A variety of RC designs, including porous polymers,⁸ ceramics,⁹ and paints,^{25,26} have employed scattering media to achieve higher solar reflectances than metal mirrors. However, the intrinsic TIR absorptivity of these materials, and morphologies that do not lend to TIR scattering, render them broadband thermal emitters. In addition to addressing this challenge, determining to what extent ultrabroadband reflectance is realistically possible by multiple light scattering – and whether that could be coupled with intrinsic absorption of constituents to achieve selective emittance – remains an important question for advancing radiative thermoregulation, and more broadly, optical design.

In this work, we propose random photonic media featuring layered, multiscale light scatterers to simultaneously achieve ultrabroadband solar-to-TIR reflectance and selective emittance in the intermediate LWIR band (**Figure 1a**). Based on theoretically guided optical design, we develop a selective LWIR emitter consisting of a nanoporous poly(4-methyl-1-pentene) (nPMP) bonded to a

microfibrous polypropylene (μ PP) underlayer, which achieves a notable solar reflectance ($R_{solar}=0.97\pm 0.01$), LWIR emittance ($\epsilon_{LWIR}=0.88\pm 0.02$), and LWIR selectivity ($\eta=\epsilon_{LWIR}/\epsilon_{TIR}=1.42\pm 0.04$) (**Figure 1b**). To our knowledge, this nPMP- μ PP is the first scattering and first polymeric media to achieve such spectral functionalities without the aid of broadband reflectors like metals and bulk ceramics (**Figure 1c**, Tables S1 and S2).

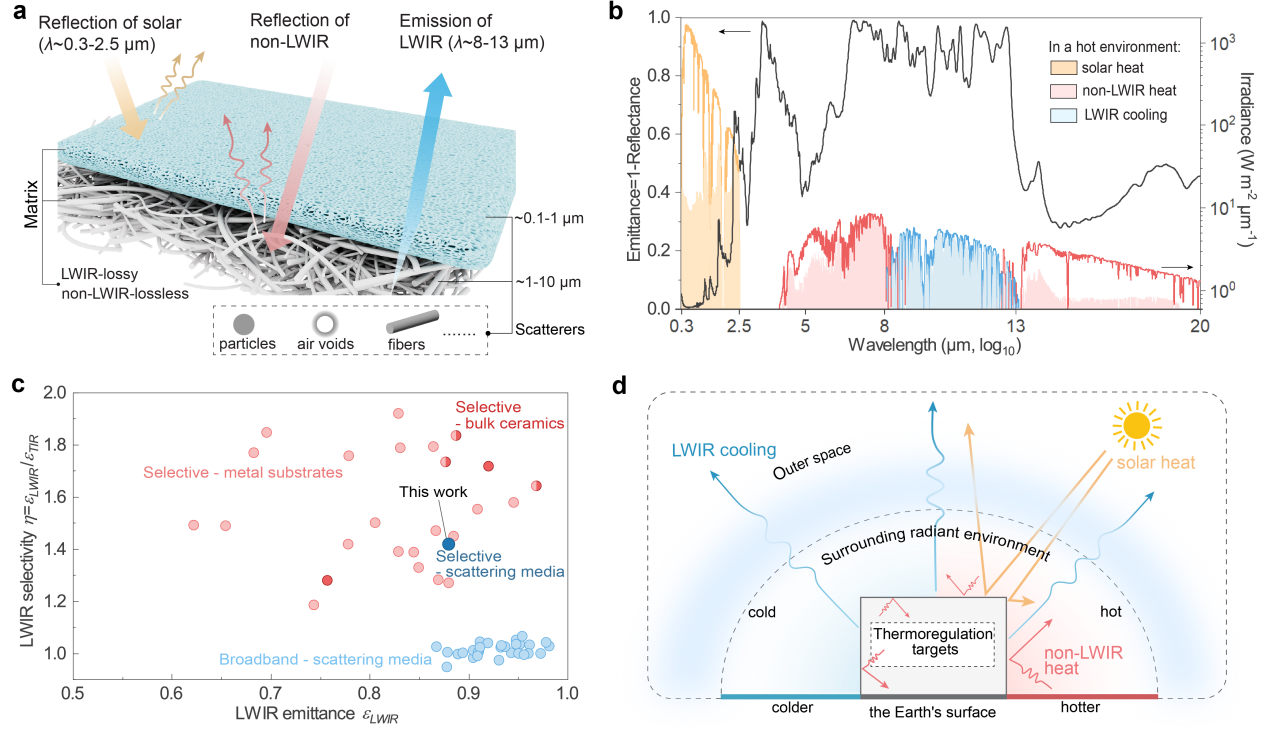


Figure 1. An ultrabroadband scattering medium with selective LWIR emission for radiative thermoregulation. (a) Schematic diagram of the proposed scattering medium, featuring a layered, multiscale structure to achieve ultrabroadband solar-to-far-infrared reflectance and selective long-wave infrared (LWIR) emittance. (b) Spectral emittance (1-reflectance) of the nPMP- μ PP selective emitter developed in this work. The color regions indicate how the nPMP- μ PP reshapes irradiance spectrum in a hot environment compared to broadband emitters: rendering solar irradiance intensity to the order of thermal irradiance; reducing non-LWIR heat gains; allowing LWIR cooling. (c) Comparisons of LWIR emittance ϵ_{LWIR} and LWIR selectivity $\eta = \epsilon_{LWIR} / \epsilon_{TIR}$ between the nPMP- μ PP and other radiative cooling materials reported in literature (Tables S1 and S2). (d) Compared to broadband emitters, selective LWIR emitters maintain radiative cooling to the sky, while blocking unwanted non-LWIR radiative heat gains or losses due to temperature variations of the surrounding environments. This can be used to thermoregulate targets such as buildings and human beings.

Through field tests validated against theoretical predictions, we further demonstrate superior passive radiative thermoregulation relative to conventional solar-reflective, broadband-emissive scattering media across diverse scenarios. This arises from the low emittance outside the LWIR further reduces unwanted radiative heat gains or losses driven by temperature variations in the nearby outdoor environment (**Figure 1b** and **d**). Deployed as a sky-facing surface, nPMP- μ PP reaches sub-ambient temperatures under intense sunlight, limited atmospheric transparency, and strong convective heat transfer, delivering higher net cooling power than a broadband RC with equally high R_{solar} . The benefit is more pronounced for vertical surfaces during both hot daytime with either strong or weak sunlight and cold nighttime, as the nPMP- μ PP further reduces non-LWIR thermal radiative heat gains or losses by $\sim 10\text{-}30\ \text{W}\cdot\text{m}^{-2}$. Thermal and energy simulations indicate that, compared with

broadband RCs, walls clad with nPMP- μ PP can enable cross-seasonal building energy savings comparable to those achieved by painting dark roofs white. When used as architectural fabrics, nPMP- μ PP can reduce heat gains into enclosed, lightweight-shielded spaces by >80%, effectively shielding humans from outdoor thermal stresses. Promisingly, established fabrication and tunability of the scattering-based design make it compatible with industry-scale production at low material cost (\sim US\$3 m⁻²), and provides a platform for tailoring solar reflectance and thermal emittance to applications in different climates. Together, these results show a practical way to harness optical scattering media towards feasibly improving passive thermoregulation of buildings, shelters, and human beings.

Optical Design of The Layered Multiscale Scattering Medium

Achieving Thermal Infrared Reflection with Scattering Media

While random photonic media comprising particles,^{25,27,28} air voids,^{8,9} or fibers have been widely explored to achieve ultrahigh R_{solar} , extending their utility to the TIR band remains largely unexplored. A critical reason is that most materials are intrinsically TIR-absorptive due to plasmonic resonances, molecular vibrations, or phonon resonances.⁶ Of the few materials that are transparent, most are unsuitable due to their weatherability (e.g., sodium chloride) or cost (e.g., diamond). However, lower order polyolefins, e.g., polyethylene (PE), polypropene (PP), and poly(4-methyl-1-pentene) (PMP), are exceptional in this regard (**Figure 2a**). The relatively simple molecular structure of PE has only a few, weak IR vibrational modes, making it highly transparent across much of the TIR band.²⁹ For PP and PMP, the saturated hydrocarbon functional groups linked by -C-C- backbone(s) have vibrational modes primarily in the LWIR, while being transmissive across most of the non-LWIR wavelengths.¹⁰ Although these properties of polyolefins have been utilized for developing TIR-transparent materials and radiative cooling applications,²⁹⁻³¹ their use as TIR scattering media has not yet been studied.

Given their ready availability and high processibility, we envisioned porous scattering media with polyolefins ($n\sim 1.5$) as the high-index component, and air ($n=1$) as the low-index component. Based on the measured refractive indices (Fig. S3), we first explored scatterer geometries that could yield the desired broadband TIR scattering (Note S1). For both spherical PP fibers and particles, the results indicate diameters d ranging between 4-16 μm could simultaneously yield desirable TIR scattering (Q_{sca}) and LWIR absorption (Q_{abs}) efficiencies (**Figure 2b** and Fig. S4). PE scatters with such sizes can also exhibit strong scattering of TIR light, but their Q_{abs} peaks at ~ 7 and ~ 14 μm and are much weaker in the LWIR (Fig. S5). Therefore, PP-based scattering media could be a better choice for making selective LWIR emitters, while PE-based ones could potentially achieve higher total TIR reflectance. Accordingly, we further investigated scattering media made of μm -sized PP scatterers using finite-difference-time-domain (FDTD) electromagnetic simulations (Note S2). A 300- μm -thick scattering medium, comprising randomly packed particles with a normal diameter distribution of 10 ± 6 μm and a volume fraction of 60%, was simulated as a representative case (**Figure 2c** and Fig. S6). Results show that when irradiated with unpolarized TIR light ($\lambda\sim 4$ -20 μm), the medium strongly reflects non-LWIR wavelengths ($\lambda\sim 4$ -6.5 μm and 13-20 μm) but exhibits low reflectance and high absorptance in the LWIR (**Figure 2d-e**). Higher reflectance, especially in the far-infrared (FIR) wavelengths, can be realized by further increasing medium thickness. This reflectance arises primarily from the fiber size, as reducing the scatterer sizes to $\sim 2\pm 1.5$ μm results in much weaker reflection of FIR light (Fig. S7). Three-dimensional simulations of a 300- μm -thick microporous PP

film also show similar optical behaviors (Fig. S8). Collectively, these results indicate that by tailoring the microstructure and material composition of random photonic media, multiple light scattering can enable broadband TIR reflection, thereby providing a new avenue for radiative thermoregulation materials.

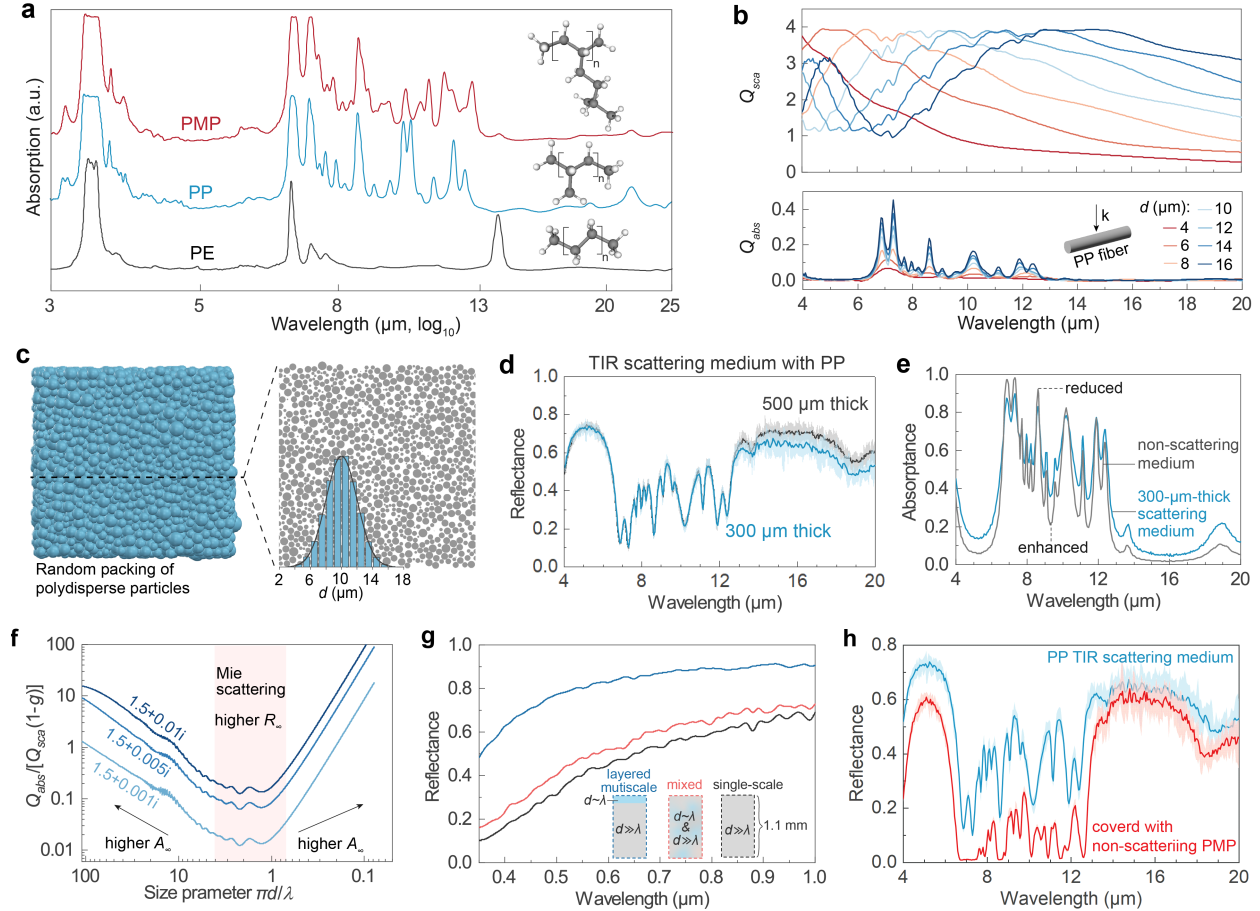


Figure 2. Optical design. (a) Absorption spectra of polymer thin films including polyethylene (PE), polypropylene (PP), and poly(4-methyl-1-pentene) (PMP). (b) Scattering efficiency Q_{sca} and absorption efficiency Q_{abs} of PP fibers with different diameters d . (c) Visualization of a random packing of polydisperse microparticles and its cross section, which is used for simulating the random scattering medium having scatters with an average diameter of 10 μm and a volume fraction of 60%. Insert: particle size distribution diagram. (d) Simulated reflection spectra of the PP-based TIR scattering medium at thicknesses of 300 μm and 500 μm . (e) Simulated absorption spectra of the 300- μm -thick TIR scattering medium made with PP, in comparison with a 300- μm -thick effective medium with the same volume fraction of PP but exhibits no TIR scattering. (f) $Q_{abs}/[Q_{sca}(1-g)]$ as the function of particle size parameter $\pi d/\lambda$, assuming the particle has a refractive index of 1.5 but different extinction coefficients. (g) Simulated reflection spectra in visible waveband for a thick scattering medium with different configurations of scatters (Fig. S10). (h) Simulated reflection spectrum in the TIR for a 300- μm -thick PP scattering medium covered with/without a nanoporous PMP film (Fig. S11).

Enhancing Ultrabroadband Functionalities by a Layered Multiscale Design

However, the competition between light absorption and reflection within scattering media prevents a single TIR-scattering layer from functioning also as an effective selective LWIR emitter (Note S3). This is because firstly, strong scattering enhances diffuse reflection near the top surface, thereby capping the maximum attainable absorptance (emittance) A_∞ at infinite thickness, even when the

material has a large extinction coefficient κ .³² This optical behavior is evident from our comparison of the absorptance of a PP-based TIR scattering medium with that of a non-scattering slab of the same thickness and volume fraction (**Figure 2e**). For example, at $\lambda \sim 8.6 \mu\text{m}$, the absorptance of the TIR-scattering medium is lower, while further increasing its thickness neither enhances absorptance nor reduces reflectance (**Figure 2d, e** and Fig. S9). Moreover, polyolefins like PP still have relatively low κ in some LWIR wavelengths (Fig. S3). In such weak-absorption regions (e.g., $\lambda \sim 9.35 \mu\text{m}$), although multiple scattering can increase absorptance at a finite thickness (**Figure 2e**), the high reflectance of >0.5 indicates a moderate A_∞ .

Another important limitation arises in the solar waveband. In principle, an optically thick scattering medium containing μm -sized scatterers should be also capable of reflecting shortwave sunlight strongly ($\lambda \lesssim d$), if they are perfectly lossless. In practice, most solar-transparent materials, including PP, have interband absorption tails and impurity absorptivity in the ultraviolet-to-visible (UV-VIS) spectral region.^{6,33} To maximize reflectance R_∞ , the intrinsically weak absorption of materials needs to be suppressed by enhancing backward scattering, i.e., minimizing the absorption to backscattering ratio $Q_{abs}/[Q_{sca}(1-g)]$ (Note S3). However, scatterers that efficiently work in TIR region are much larger than solar wavelengths ($\lambda \ll d$), having notably lower Q_{sca} and higher $Q_{abs}/[Q_{sca}(1-g)]$ compared to the Mie scattering regime ($\lambda \sim d$) (**Figure 2f**). This increases absorptance and reduces R_∞ , and may explain why some previously reported microporous media exhibit less UV reflectance despite being quite thick.^{9,34} In other words, using a mixture of scatterers with a very broad distribution in d may not be optimal for ultrabroadband reflectance.

These theoretical considerations led us to anticipate that a scattering medium made from layers of scatterers at different size regimes is essential to simultaneously achieve high, ultrabroadband reflectance and selective emittance. For the case of selective LWIR emitters (**Figure 1b**), the bottom layer should consist of scatterers with d at the orders of 1-10 μm to reflect TIR light, and the top layer should be made with scatterers with d confined to the submicron regime ($d \sim 0.1-1 \mu\text{m}$). As our optical simulations show, the strong scattering of UV-VIS light by the small-sized scatterers in the top layer can substantially enhance solar reflectance; by contrast, when only large-sized scatterers are present or when they are mixed with small-sized ones, the reflectance remains limited even for thick layers (**Figure 2g** and Fig. S10). In the LWIR where $d \ll \lambda$, the negligible scattering by the top layer enhances absorptance when the medium is absorptive and thick enough. To this end, we chose a nanoporous PMP on top of the PP-based TIR scattering underlayer. This is because like PP, PMP is highly transparent outside the LWIR, while inside the LWIR, PMP's intrinsic absorption peaks partially complement those of PP (**Figure 2a** and Fig. S3). Moreover, the low effective refractive index of a nanoporous layer can reduce Fresnel reflectance at the air interface. Our simulations show that when a 500 μm -thick nanoporous PMP film is used, ϵ_{LWIR} increases from 0.61 to 0.89 (**Figure 2h** and Fig. S11), and LWIR selectivity η reaches ~ 1.45 (here defined within the 4-20 μm simulation bandwidth).

Material Fabrication and Characterization

Having established a theoretical basis for the polyolefin-based layered, multiscale scattering medium, we considered pathways to fabricate it at scale. Promisingly, microfibrous and porous polymers, including polyolefins, are already manufactured at scale for many industrial products like separators, filters, and fabrics. Our initial study of such commercially available products showed that some variants indeed exhibit modest, but hitherto unexploited TIR scattering (Fig. S12), with non-woven

PP fabrics being particularly promising. In principle, processes like melt extrusion and spinning used to manufacture such variants could be tailored to create microfibrous polyolefins with fiber sizes optimized for scattering TIR radiation.³⁵ Here in this work to demonstrate a proof of concept with a potential for immediate impact, we custom-ordered a melt-blown microfibrous polypropylene (μ PP) fabric.³⁶ While not precisely tailored, the nonwoven μ PP fabric has a suitable microstructure, featuring randomly oriented PP fibers with diameters ranging from 2 to 18 μm (**Figure 3a-b** and Fig. S13). Optical measurements show that the μ PP, at a thickness of $\sim 500\ \mu\text{m}$ and weight of $\sim 0.15\ \text{kg m}^{-2}$, is indeed an ultrabroadband UV-to-FIR reflector and a wideband LWIR emitter, with $R_{\text{solar}} \sim 0.91$, $\epsilon_{\text{LWIR}} \sim 0.51$, $\epsilon_{\text{non-LWIR}} \sim 0.33$ at near-normal incidence (**Figure 3c**).

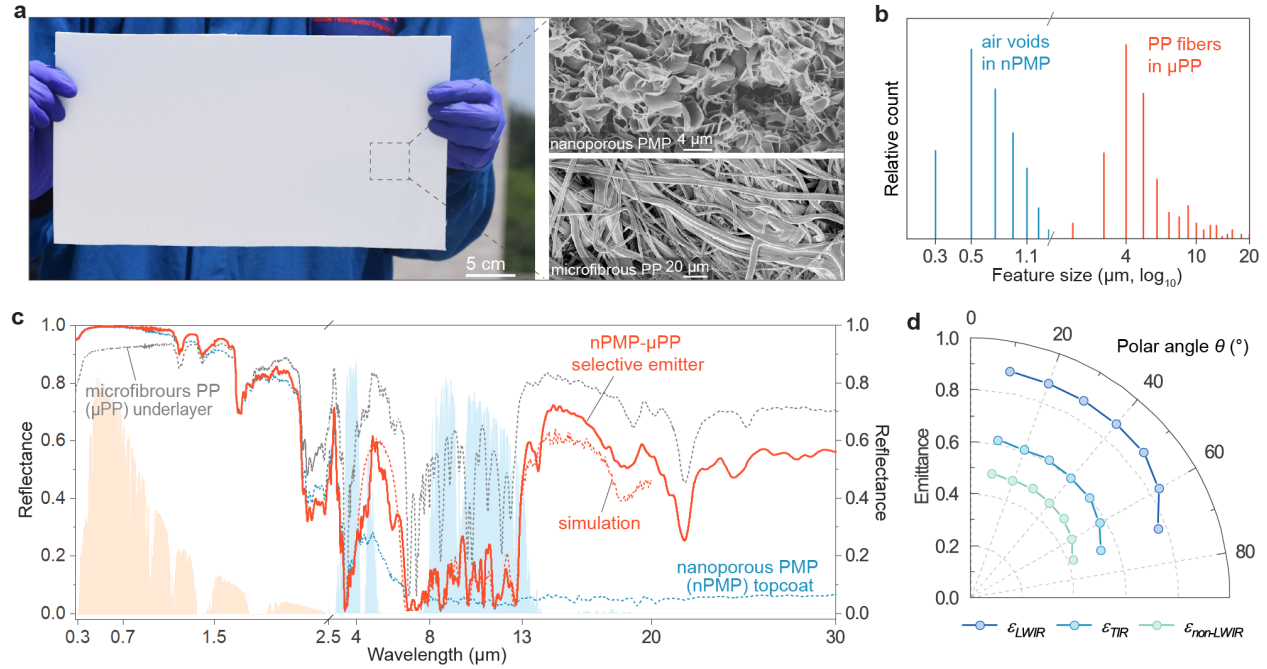


Figure 3. Characterization of nPMP- μ PP. (a) Photograph of a $\sim 40 \times 20\ \text{cm}^2$ nPMP- μ PP selective emitter sample and the micrographs of the nPMP topcoat (showing random PMP lamellae and air voids) and the nonwoven μ PP fabric underlayer (showing random PP microfibrils). (b) Size distributions of air voids within the nPMP and fibers within the μ PP. (c) Measured spectral reflectance the nPMP- μ PP selective emitter at near-normal incidence, and the constituent 500- μm -thick nPMP topcoat and the 500- μm -thick μ PP underlayer. The simulated TIR reflectance of a 500- μm -thick nPMP on 300- μm -thick μ PP is also plotted as comparison. Plotted against ASTM G173 Global solar spectrum (yellow) and the TIR atmospheric transmittance for mid-latitude summer conditions (light blue). (d) LWIR, TIR and non-LWIR emittance of the nPMP- μ PP selective emitter as a function of angle.

However, strong TIR scattering by the PP fibers limits μ PP's ϵ_{LWIR} . Besides, solar reflectance, while high, falls in the shorter solar wavelengths (Fig. S14), as predicted by our theoretical analysis. Thus, guided by the optical design, we experimentally deposited a nanoporous PMP (nPMP) topcoat on the μ PP using a scalable phase inversion (immersion-precipitation) method.³⁷ The process involves casting a film of a PMP-cyclohexane dope solution onto the substrate, followed by immediate immersion in isopropanol as the nonsolvent. The rapid solvent-nonsolvent exchange microstructures the PMP into petal-like lamellae, creating within minutes numerous interstitial voids with an average size of $\sim 0.5\ \mu\text{m}$ (**Figure 3a-b** and Fig. S15). These features act as Mie scatterers of sunlight, causing a 160 μm -thick nPMP film to attain $R_{\text{solar}} > 0.91$, and > 0.95 when placed on the μ PP (Fig. S16). By

comparing the optical characteristics at different nPMP thicknesses (Fig. S17), the final nPMP- μ PP selective emitter was chosen to comprises a ~ 500 μm -thick nPMP topcoat on a ~ 500 μm -thick μ PP underlayer, which yields high $R_{\text{solar}}=0.97\pm 0.01$, $\varepsilon_{\text{LWIR}}=0.88\pm 0.02$, and notable $\eta=1.42\pm 0.04$ at near-normal incidence (**Figure 3c** and Fig. S17). The agreement of such optical properties with our optical design verifies that the size scales and materials of scatterers can be synergistically optimized to realize complex spectral functionalities. Moreover, because of the scattering-based optical mechanism and low effective index of the nPMP topcoat, the selective emittance extends across a wide angular range (**Figure 3d**), yielding hemispherical $\varepsilon_{\text{LWIR}}$ of ~ 0.85 and η of ~ 1.45 . We use this design for subsequent investigations.

Evaluation of Thermal Performance

The high solar reflectance and selective LWIR emittance of nPMP- μ PP enable it to achieve notable radiative thermoregulation relative to broadband emitters across a range of scenarios. We substantiated this through a series of field tests comparing the steady-state temperatures of and heat flows through nPMP- μ PP samples relative to two broadband controls (Fig. S18). The first control is a commercial white paint, served as a typical benchmark ($R_{\text{solar}}=0.83$, $\varepsilon_{\text{LWIR}}=0.94$, $\eta=1.03$). The second is a broadband RC with the same underlayer as nPMP- μ PP, but with nPMP replaced by an equivalent thickness of expanded polytetrafluoroethylene (ePTFE), yielding nearly identical $R_{\text{solar}}=0.96$ and $\varepsilon_{\text{LWIR}}=0.88$ to nPMP- μ PP, but a broadband emittance ($\eta=0.99$). Comparison with the ePTFE- μ PP therefore parses out the effect of selective emittance. The tests were conducted with samples in sky-facing or vertical orientations and in urban or semi-urban environments, during summer days with and without direct sunlight, and during winter nights. Notably, rather than being shielded from thermal convection by windshields as in many previous studies, all samples were fully exposed to ambient conditions. Furthermore, each sample was mounted on a steel backplate to increase thermal capacity and insulated from the rear to suppress parasitic heat flows (**Figure 4a**).

Skyward Radiative Cooling Under Harsh Conditions

Sky-facing radiative cooling tests were conducted in Princeton (New Jersey, USA) during the summer of 2025, when strong sunlight, sporadic cloud cover, warm ambience, periodic winds, and high total precipitable water (TPW) made sub-ambient radiative cooling particularly challenging. Over a 4-hour period on June 5 afternoon with a peak/mean solar irradiance I_{solar} of 1000/840 W m^{-2} , TPW of ~ 28 mm and average wind speed of ~ 4 m s^{-1} , the nPMP- μ PP selective emitter stayed $\sim 4.9/4.0^\circ\text{C}$ (peak/mean) cooler than the white paint, $2.4/1.6^\circ\text{C}$ cooler than ambient air, and $0.8/0.5^\circ\text{C}$ cooler than the ePTFE- μ PP broadband RC (**Figure 4b,c**). Notably, this cooling was achieved when the combination of high TPW and scattered clouds partially closed the atmospheric transparency window and raised the radiant temperature T_{radiant} of sky to within 12°C of the ambient temperature T_{amb} . As a benchmark, under such conditions the maximum attainable average radiative cooling power \bar{P}_{cooling} for a near-ideal broadband RC ($R_{\text{solar}}=0.97$, $\varepsilon_{\text{LWIR}}=1$, $\eta=1$) is ~ 47 W m^{-2} when it is at T_{amb} . We calculated \bar{P}_{cooling} of the samples tested (Note S4): whereas the white paint achieved a net radiative heat gain of ~ 57 W m^{-2} , the broadband RC and nPMP- μ PP samples achieved average radiative cooling of ~ 27 and ~ 40 W m^{-2} respectively, under steady-state temperatures (**Figure 4c**). If the emitters were held at T_{amb} , the \bar{P}_{cooling} of nPMP- μ PP would have been ~ 50 W m^{-2} , 17 W m^{-2} higher than that of ePTFE- μ PP.

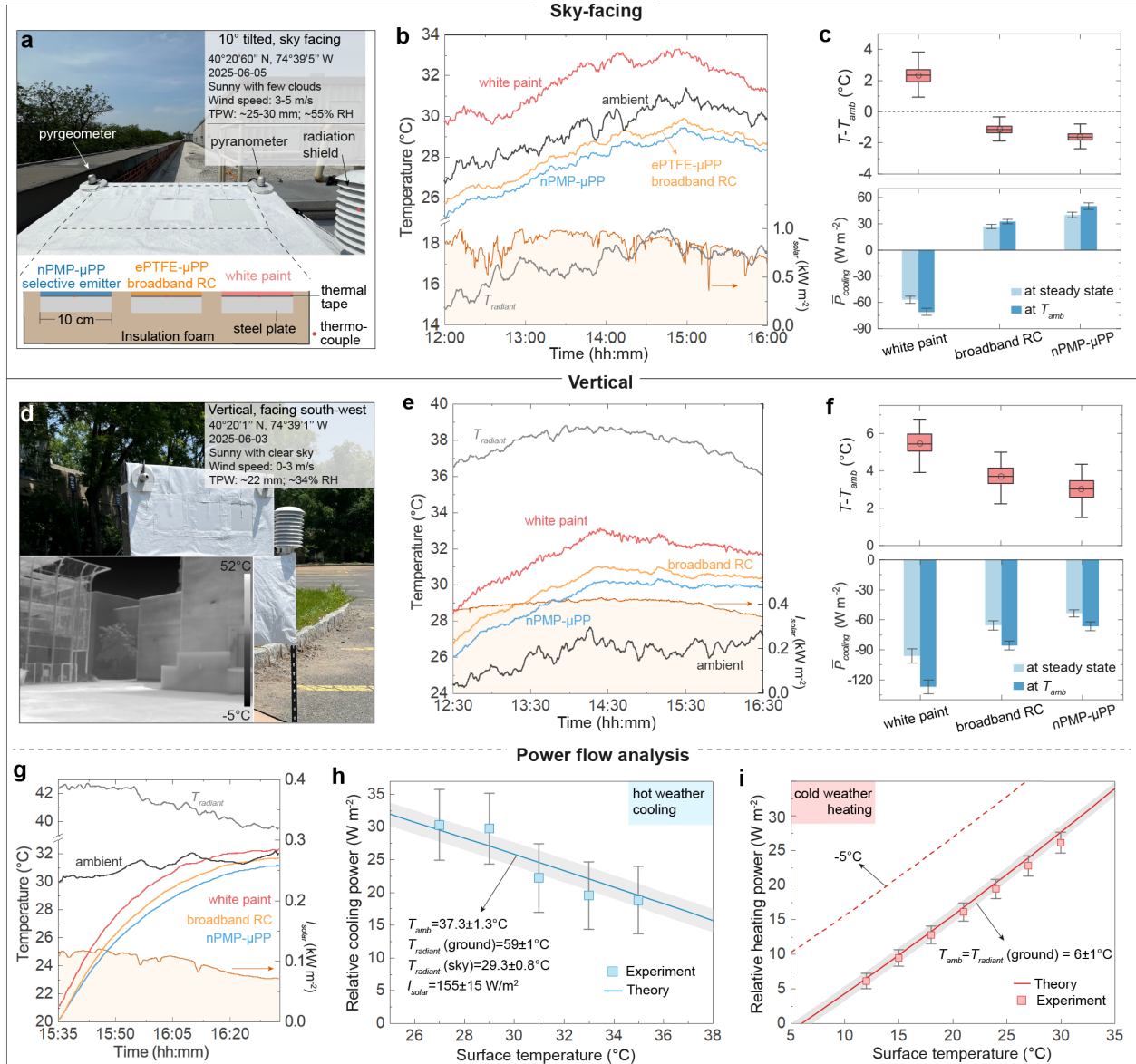


Figure 4. Field tests of thermoregulation performance. (a-c) When samples are horizontally placed facing the sky: (a) photograph and schematic of the field test setup; (b) real-time temperature data, TIR irradiance expressed in radiant temperature T_{radiant} , and solar irradiance I_{solar} ; (c) box-plot of the sample temperature T relative to ambient temperature T_{amb} , and the average radiative cooling power P_{cooling} when samples are either steady-state or assumed to be at T_{amb} . (d-f) When samples are vertically placed facing both sky and terrestrial environment: (d) photograph of the field test setup and a thermal photo showing the radiant environment in the field of view; (e) real-time temperature data, TIR irradiance expressed in T_{radiant} , and solar irradiance I_{solar} ; (f) box-plot of the sample temperature T relative to ambient temperature T_{amb} , and the average radiative cooling power P_{cooling} when samples are either steady-state or assumed to be at T_{amb} . (g-i) Differential power flow analysis in vertical orientation: (g) field test results when samples were vertically placed in a hot terrestrial environment without direct sunlight and were heated by the environment; (h) radiative heat gains prevented (i.e., relative cooling) in a hot environment; (i) radiative heat losses prevented (i.e., relative heating) in a cold environment by the nPMP- μ PP compared to the ePTFE- μ PP. Note: T_{amb} is averaged with a moving 5-minute window, while the other temperature data are one-minute average.

Additional tests conducted under other weather conditions yielded similar results, including on 23 June during a heat-dome event³⁸ that produced extremely hot (T_{amb} up to $\sim 37^\circ\text{C}$) and humid weather

(TPW up to ~ 35 mm) (Fig. S19). Between 08:00 and 16:00 on that day, while the maximum attainable $\bar{P}_{cooling}$ of a near-ideal broadband RC was only ~ 25 W m $^{-2}$, the nPMP- μ PP selective emitter attained average cooling of 4.3°C, 2.1°C and 0.4°C relative to white paint, ambient air, and broadband RC, respectively. Overall, these results highlight how the high solar reflectance and selective LWIR emittance of nPMP- μ PP effectively suppresses radiative heat gains, enabling sky-facing variants to remain sub-ambient even when environmental conditions are non-ideal for radiative cooling.

Radiative Thermoregulation in Vertical Orientation

While radiative cooling of sky-facing emitters has been long explored, the ability of selective emitters to thermoregulate vertical surfaces relative to broadband emitters – i.e., relative cool in hot weather and heat in cold weather – has only been recently elucidated.^{10,13} When vertically oriented and facing the hot thermal environments experienced by building facades and human bodies in urban settings, the cooling benefits of the nPMP- μ PP selective emitter become even more pronounced. In contrast to the sky-facing configuration, where the $T_{radiant}$ was lower than T_{amb} (**Figure 4a**), vertically oriented samples were exposed to warm ground and surrounding buildings, leading to elevated TIR irradiance with $T_{radiant} \sim 12^\circ\text{C}$ higher than T_{amb} during the field test (**Figure 4d** and Fig. S20). This corresponds to over 70 W m $^{-2}$ of net TIR heat load, forcing the highly solar-reflective but broadband emissive ePTFE- μ PP to remain $\sim 3.7^\circ\text{C}$ above T_{amb} on average (**Figure 4e**). The white paint, owing to its lower solar reflectance, was $\sim 5.5^\circ\text{C}$ above T_{amb} . By reducing TIR terrestrial heat gain from the environment relative to the broadband RC, and also solar heat gain relative to the white paint, nPMP- μ PP stayed $\sim 0.7^\circ\text{C}$ and $\sim 2.5^\circ\text{C}$ cooler relative to the two emitters (**Figure 4f**). Similar trends were also observed under other warm outdoor conditions (Fig. S21). The relative cooling performance in such conditions is similar to those of metallized selective emitters.¹⁰

Because vertical surfaces receive substantially more non-LWIR irradiation but less direct solar irradiation than horizontal surfaces, the selective LWIR emission of nPMP- μ PP plays a more critical role in thermoregulation. This was demonstrated in a test with samples exposed to a hot terrestrial environment but only diffuse sunlight ($I_{solar} \sim 100$ W m $^{-2}$), showing that only nPMP- μ PP remained cooler than ambient air after 1 h of heating by the surrounding environment (**Figure 4g**). Analysis of the temperature rise confirmed that nPMP- μ PP absorbed notably less radiant heat (Fig. S22), and since solar absorption differences were less than 2 W m $^{-2}$, the observed cooling is primarily attributed to reduced absorption of non-LWIR terrestrial irradiation.

We further performed field tests and detailed power flow analysis to quantify this effect (Note S5). Under a hot condition, with T_{amb} of $\sim 37.3^\circ\text{C}$ and the $T_{radiant}$ of ground reaching $\sim 60^\circ\text{C}$ (Fig. 23), both theoretical calculations and experimental measurements showed that nPMP- μ PP attained a relative cooling power of ~ 30 W m $^{-2}$ at 27°C and ~ 17 W m $^{-2}$ at T_{amb} compared with the ePTFE- μ PP broadband RC (**Figure 4h**). Notably, at representative human-body surface temperatures of 32-35 °C, the relative cooling still exceeded 20 W m $^{-2}$. Moreover, under cold conditions such as winter nights, when building surfaces and human bodies lose substantial heat to the environment, nPMP- μ PP's low emittance in the non-LWIR also enabled reduced radiative heat loss and relative heating effect (**Figure 4i** and Fig. S24). For building surfaces, which can be as much as 10-15°C warmer than the terrestrial environment in the winter, we observed relative heating of 10-15 W m $^{-2}$ when T_{amb} was $\sim 6^\circ\text{C}$, and at human-body surface temperatures, the relative heating was ~ 30 W m $^{-2}$. Notably, these results are largely consistent with theoretical predictions. The magnitude of the relative cooling or heating

power increases with the temperature difference between the thermoregulating surface and the surrounding radiant environment, by $\sim 1.2 \text{ W m}^{-2}$ per degree Celsius.

Potential Impact

Deployability

Our work demonstrates that a selective LWIR emitter, which provides superior passive thermoregulation compared to more common broadband emitters, can be realized entirely using scattering media. This could offer broad utility and distinct advantages, including low cost and high scalability, thereby facilitating the practical deployment of spectrally selective radiative heat control. Preliminary analysis of the proof-of-concept nPMP- μ PP suggests that the cost can be constrained to \sim US\$3 m^{-2} (Table S3 and S4). This is notably lower than the cost of many other selective LWIR emitters, and could be further reduced when totally using established industrial manufacturing process for microfibrinous polymers that are solvent-free (Fig. S25),³⁶ being comparable with other scattering-media designs like paints and fabrics.^{25,28} Moreover, the appearance of scattering media can be readily tuned by incorporating colorants (Fig. S26), while eliminating metals avoids glare and may mitigate weathering-induced degradation of optical properties. The porous morphology and metal-free composition also impart flexibility and breathability without compromising waterproofness, expanding the range of potential applications (Fig. S27). Although the focus of this work is on optical design, we note that a key engineering challenge is to improve durability under prolonged outdoor exposure in relevant applications, as polyolefins are often susceptible to chemical damage by UV irradiation. An accelerated UV aging of the nPMP- μ PP under intensity of 350 W m^{-2} for one week (equivalent to ~ 6 months outdoor considering a 400 MJ m^{-2} yearly exposure) shows little impact on its optical performance (Fig. S28). Potential improvement pathways include incorporating UV stabilizers that are also spectrally selective or have little impact on TIR optical properties.^{39,40} Besides, we note here that the nature of our optical design means that the nPMP topcoat, and if needed, also the μ PP TIR-scattering underlayer, could in principle be replaced with other LWIR-selective or TIR-lossless materials featuring high UV stability, especially those can be processed into scattering media consisting of particles, fibers, or porous networks.^{10,41–45}

Along with the demonstrated radiative cooling and thermoregulation performance relative to traditional designs, these attributes present possibilities for all-season building energy savings and improving thermal comfort, as discussed below.

Building Envelopes for Energy Efficiency

Cooling-energy savings associated with highly solar-reflective, LWIR-emissive roofs are well documented.^{9,46,47} While a selective emitter does enable better radiative cooling than a broadband emitter, the improvement is often modest at best for sky-facing surfaces.⁴⁸ Nonetheless, the overall cooling benefit remains substantial, and in the case of our design, achievable by overcoming the design limitations and cost of metal-based selective LWIR emitters reported thus far. A recently demonstrated, and potentially more impactful opportunity lies in the thermoregulation of facades that see the terrestrial environment,¹⁰ where the nPMP- μ PP's optical properties provide both cooling in hot weather and heating in cold weather relative to broadband emitters (**Figure 4h, i**). Also, walls are often less insulated and present larger surfaces than roofs. Therefore, here we focus on the energy-saving potential for facade thermoregulation using a building thermal model with the

capability of simulating spectral selective facades (Note S6). We evaluated the energy savings for a mid-sized building in three cities representing distinct climate regimes (**Figure 5a**). The building was assumed to have either wooden walls with R13 insulation, as is common in the US, or brick walls, as is often the case in the global south.

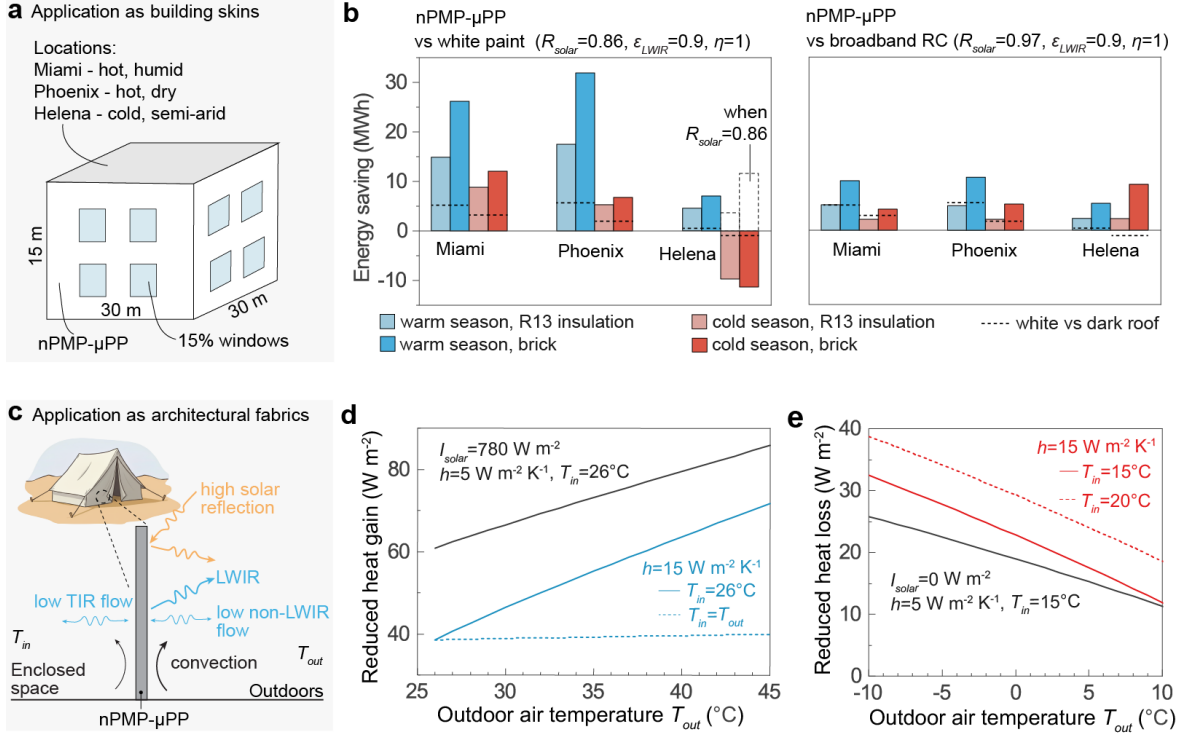


Figure 5. Potential impact on improving energy saving and thermal comfort. (a) Schematic of the mid-size residential building for modelling energy saving performance on walls. (b) Energy savings achieved in three cities representing distinct climate regimes, relative to a typical white paint and a broadband radiative cooler. (c) Schematic of heat flows through the nPMP- μ PP as an architectural fabric that enables strong reflection of solar heat, reduced non-LWIR heat exchange with terrestrial environment, and reduced TIR heat exchange with the indoor environment. This significantly reduces (d) heat gains by the enclosed space in hot weather (e.g., summer daytime), and (e) heat loss in cold weather (e.g., winter nighttime). h : outdoor convective coefficient; T_{in} : indoor temperature.

When benchmarked against typical white surfaces ($R_{solar}=0.86, \epsilon_{LWIR}=0.9, \eta=1$), exterior wall envelopes made from nPMP- μ PP reduce cooling and heating loads across warm and hot climates, enabling ~ 22 - 39 MWh annual energy savings and CO_2 reductions exceeding ~ 5 - 9 tons (**Figure 5b**). This often surpasses the well-documented benefits associated with painting dark roofs white.⁴⁶ In cold-climates regions like Helena, the ultrahigh R_{solar} of nPMP- μ PP introduces a penalty due to overcooling in winter; however, it still outperforms broadband RCs with comparable R_{solar} ($R_{solar}=0.97, \epsilon_{LWIR}=0.9, \eta=1$) (**Figure 5b**), highlighting the intrinsic advantage of spectrally selective TIR emission. Crucially, with the design of layered scattering media, R_{solar} and ϵ_{TIR} can be decoupled and tuned, e.g., by introducing colorants to reduce R_{solar} while largely preserving TIR properties (Fig. S26), and by adjusting the dosage of the top layer to adjust ϵ_{LWIR} (Fig. S17). Simulations show that a darker, LWIR-selective variant ($R_{solar}=0.86, \epsilon_{LWIR}=0.88, \eta=1.42$) retains notable energy savings across both hot and cold climates (up to ~ 10 MWh for brick walls, Fig. S29). Moreover, since the μ PP underlayer has a selective but lower ϵ_{LWIR} of 0.51 and ϵ_{TIR} of 0.39, if used solely by itself to enhance the reduction in TIR

heat loss in heating-dominated conditions, it may substantially improve energy efficiency by ~ 10 MWh with a modest R13 insulation (Fig. S29). Together, these results indicate our scattering-based design could be conveniently tailored and thus provides a flexible platform for engineering materials with application-specific radiative regulation functionalities.

Wearable and Architectural Fabrics

Radiative thermoregulation can also directly enhance human thermal comfort in minimally sheltered settings or under outdoor exposure.⁴⁹ The optical design proposed in this work is compatible with polymeric fabrics,⁵⁰ thus offering a promising paradigm for thermoregulation textile engineering. While previous studies have established that textiles with high R_{solar} can effectively reduce heat stress under sunlight, their susceptibility to broadband TIR heat in urban settings has only been recently noticed.¹⁰ Our research demonstrates that nPMP- μ PP, beyond solar reflection, can further reduce undesired radiant fluxes at temperatures characteristic of clothed human bodies in both hot and cold urban environments, by ~ 20 and ~ 30 W m^{-2} , respectively (**Figure 4h, i**). These are about 20% of human body metabolic rate.⁵¹

Beyond garments, we anticipate that the LWIR-selective emissive front side, together with the low-emittance backside enabled by our design, could also be valuable for architectural fabrics. Such fabrics are typically used to provide basic shelter with minimal material usage (e.g., in tents and emergency shelters), yet conventional designs offer poor thermal insulation due to strictly limited thickness (~ 1 mm) and thermal mass.⁵² We therefore performed heat-flow calculations to gauge the thermal performance of nPMP- μ PP in such scenarios (**Figure 5c** and Note S7). Under hot conditions with solar irradiance of ~ 780 W m^{-2} and ground temperatures 20°C above outdoor T_{amb} , a vertically oriented nPMP- μ PP reduces heat gain into temperature-controlled indoors by ~ 40 - 80 W m^{-2} (**Figure 5d**). Even without indoor temperature control and indoor temperature T_{in} reaches T_{amb} , it still reduces heat gain by ~ 39 W m^{-2} , a $>80\%$ reduction over that of conventional fabrics, and comparable to increasing the thickness of conventional fabrics by ~ 75 mm. During cold nights, when T_{amb} drops to 0°C and T_{in} is maintained at the minimum recommended 15°C , nPMP- μ PP could also reduce heat loss by 23 W m^{-2} (**Figure 5e**).

Conclusions

We developed a layered, multiscale scattering medium that delivers ultrabroadband reflection from the ultraviolet to the far-infrared while enabling band-selective absorption, without relying on metals or other substrates. Leveraging this architecture, we demonstrate a fabric-like selective LWIR emitter that can radiatively insulate underlying surfaces from non-LWIR radiative heat gain (and loss) while maintaining efficient LWIR exchange with the sky. Optical and thermal analysis and experiments validate the designed spectral response and show improved passive radiative thermoregulation across diverse scenarios relative to broadband emitters. By the nature of the low cost, established scalable manufacturing, and tunability of scattering media, this strategy holds promise for advancing passive radiative heat control for building energy savings and human thermal comfort. More broadly, our results mark an advancement over prevailing mixture-based paradigm in scattering-media design,^{8,9,53} and highlight the advantage of a multiscale, layered organization of scatterers based on their intrinsic optical properties. The same design principle could be applicable to a broad range of

systems that harness multiple elastic waves scattering in complex media for controlling broadband reflection and absorption, such as coatings, energy harvesting, and camouflage.

References

1. Fan, S. Thermal Photonics and Energy Applications. *Joule* **1**, 264–273 (2017).
2. Talghader, J. J., Gawarikar, A. S. & Shea, R. P. Spectral selectivity in infrared thermal detection. *Light Sci Appl* **1**, e24–e24 (2012).
3. Dias, M. R. S. *et al.* Photonics roadmap for ultra-high-temperature thermophotovoltaics. *Joule* **7**, 2209–2227 (2023).
4. So, S. *et al.* Radiative Cooling for Energy Sustainability: From Fundamentals to Fabrication Methods Toward Commercialization. *Advanced Science* **11**, 2305067 (2024).
5. Raman, A. P., Anoma, M. A., Zhu, L., Rephaeli, E. & Fan, S. Passive radiative cooling below ambient air temperature under direct sunlight. *Nature* **515**, 540–544 (2014).
6. Palik, E. D. *Handbook of Optical Constants of Solids*. vol. 3 (Academic press, 1998).
7. Zhai, Y. *et al.* Scalable-manufactured randomized glass-polymer hybrid metamaterial for daytime radiative cooling. *Science* **355**, 1062–1066 (2017).
8. Mandal, J. *et al.* Hierarchically porous polymer coatings for highly efficient passive daytime radiative cooling. *Science* **362**, 315–319 (2018).
9. Zhao, X. *et al.* A solution-processed radiative cooling glass. *Science* **382**, 684–691 (2023).
10. Mandal, J. *et al.* Radiative cooling and thermoregulation in the earth's glow. *Cell Reports Physical Science* **5**, 102065 (2024).
11. Granqvist, C. G. & Hjortsberg, A. Radiative cooling to low temperatures: General considerations and application to selectively emitting SiO films. *Journal of Applied Physics* **52**, 4205–4220 (1981).
12. Banik, U. *et al.* Efficient Thin Polymer Coating as a Selective Thermal Emitter for Passive Daytime Radiative Cooling. *ACS Appl. Mater. Interfaces* **13**, 24130–24137 (2021).
13. Kim, D. H. *et al.* Ultra-thin and near-unity selective emitter for efficient cooling. *Opt. Express, OE* **29**, 31364–31375 (2021).
14. Berdahl, P. Radiative cooling with MgO and/or LiF layers. *Appl. Opt., AO* **23**, 370–372 (1984).
15. Wang, X. *et al.* A gradient nanoporous radiative cooling ceramic with high spectral selectivity. *Chemical Engineering Journal* **500**, 157344 (2024).
16. Trombe, F. Perspectives sur l'utilisation des rayonnements solaires et terrestres dans certaines régions du monde. *Revue Generale Thermique* **6**, 1215–1234 (1967).
17. Folgner, K. A. *et al.* Environmental durability of protected silver mirrors prepared by plasma beam sputtering. *Appl. Opt., AO* **56**, C75–C86 (2017).
18. Schiler, M. & Valmont, E. Urban Environmental Glare: the Secondary Consequence of Highly Reflective Materials. in (Geneva, Switzerland, 2006).

19. Yang, P., Chen, C. & Zhang, Z. M. A dual-layer structure with record-high solar reflectance for daytime radiative cooling. *Solar Energy* **169**, 316–324 (2018).
20. Harris, D. C. *Materials for Infrared Windows and Domes: Properties and Performance*. (SPIE Press, 1999).
21. McQueen, N., Kelemen, P., Dipple, G., Renforth, P. & Wilcox, J. Ambient weathering of magnesium oxide for CO₂ removal from air. *Nat Commun* **11**, 3299 (2020).
22. Wiersma, D. S. Disordered photonics. *Nature Photon* **7**, 188–196 (2013).
23. Wilts, B. D. *et al.* Evolutionary-Optimized Photonic Network Structure in White Beetle Wing Scales. *Advanced Materials* **30**, 1702057 (2018).
24. Yu, S., Qiu, C.-W., Chong, Y., Torquato, S. & Park, N. Engineered disorder in photonics. *Nat Rev Mater* **6**, 226–243 (2021).
25. Li, X., Peoples, J., Yao, P. & Ruan, X. Ultrawhite BaSO₄ Paints and Films for Remarkable Daytime Subambient Radiative Cooling. *ACS Appl. Mater. Interfaces* **13**, 21733–21739 (2021).
26. Felicelli, A. *et al.* Thin layer lightweight and ultrawhite hexagonal boron nitride nanoporous paints for daytime radiative cooling. *CR-PHYS-SC* **3**, (2022).
27. Atiganyanun, S. *et al.* Effective Radiative Cooling by Paint-Format Microsphere-Based Photonic Random Media. *ACS Photonics* **5**, 1181–1187 (2018).
28. Mandal, J., Yang, Y., Yu, N. & Raman, A. P. Paints as a Scalable and Effective Radiative Cooling Technology for Buildings. *Joule* **4**, 1350–1356 (2020).
29. Tong, J. K. *et al.* Infrared-Transparent Visible-Opaque Fabrics for Wearable Personal Thermal Management. *ACS Photonics* **2**, 769–778 (2015).
30. Grenier, P. Réfrigération radiative. Effet de serre inverse. *Rev. Phys. Appl. (Paris)* **14**, 87–90 (1979).
31. Leroy, A. *et al.* High-performance subambient radiative cooling enabled by optically selective and thermally insulating polyethylene aerogel. *Science Advances* **5**, eaat9480 (2019).
32. McNeil, L. E. & French, R. Light scattering from red pigment particles: multiple scattering in a strongly absorbing system. *Journal of applied physics* **89**, 283–293 (2001).
33. Zuo, X., Li, X., Wang, C., Ma, L. & Liu, L. Determination of complex refractive index of plastics from ultraviolet to mid-infrared by ellipsometry. *Infrared Physics & Technology* **134**, 104910 (2023).
34. Mandal, J. In search of the ideal radiative cooling material: the promise of porous ceramics. in *Bulletin of the American Physical Society* (American Physical Society, 2021).
35. Mather, R. Polyolefin fibres. in *Synthetic fibres: nylon, polyester, acrylic, polyolefin*. Cambridge: Woodhead Publishing 235–292 (2005).
36. Drabek, J. & Zatloukal, M. Meltblown technology for production of polymeric microfibers/nanofibers: A review. *Physics of Fluids* **31**, 091301 (2019).
37. Lai, J.-Y., Lin, F.-C., Wang, C.-C. & Wang, D.-M. Effect of nonsolvent additives on the porosity and morphology of asymmetric TPX membranes. *Journal of membrane science* **118**, 49–61 (1996).

38. NASA Earth Observatory. Sizzling Start to Summer. <https://science.nasa.gov/earth/earth-observatory/sizzling-start-to-summer-154475/> (2025).
39. Christmann, J., Gardette, J.-L., Pichon, G., Bouchut, B. & Therias, S. Photostabilization of polyethylene by a hindered amine light stabilizer in blooming conditions and impact of MDO processing. *Polymer Degradation and Stability* **191**, 109683 (2021).
40. *Poly IR Fresnel Lenses for Infrared Wavelengths*. <https://www.fresneltech.com/hubfs/Spec Sheets/POLYIR Brochure.pdf?hsLang=en>.
41. Li, D. *et al.* Scalable and hierarchically designed polymer film as a selective thermal emitter for high-performance all-day radiative cooling. *Nat. Nanotechnol.* **16**, 153–158 (2021).
42. Piperno, S., Lozzi, L., Rastelli, R., Passacantando, M. & Santucci, S. PMMA nanofibers production by electrospinning. *Applied Surface Science* **252**, 5583–5586 (2006).
43. Bao, H. *et al.* Double-layer nanoparticle-based coatings for efficient terrestrial radiative cooling. *Solar Energy Materials and Solar Cells* **168**, 78–84 (2017).
44. Raza, A., Alketbi, A. S., Askar, K. & Zhang, T. Single layer broadband spectrally selective SiON coatings for passive radiative cooling. *Applied Physics Letters* **124**, 192201 (2024).
45. Liu, H. *et al.* Preparation of silicon-nitride ceramic fibers with hafnium compounds loaded on the surface and the high temperature properties. *Vacuum* **220**, 112732 (2024).
46. Baniassadi, A., Sailor, D. J. & Ban-Weiss, G. A. Potential energy and climate benefits of super-cool materials as a rooftop strategy. *Urban Climate* **29**, 100495 (2019).
47. Wang, N. *et al.* Performance evaluation of radiative cooling for commercial-scale warehouse. *Materials Today Energy* **24**, 100927 (2022).
48. Jin, Y. & Kats, M. A Gradient Atmospheric Model Reveals Enhanced Radiative Cooling Potential and Demonstrates the Advantages of Broadband Emitters. *Laser & Photonics Reviews* **19**, e00371 (2025).
49. Abraham, D. E. *et al.* Efficient outdoor thermal comfort via radiant cooling and infrared-reflective walls. *Nat Sustain* **8**, 642–650 (2025).
50. Tyvek® Suits | DuPont™ Tyvek® Suits | Disposable Tyvek® Suits. <https://www.dupont.com/personal-protection/tyvek-for-ppe.html#sustainability>.
51. Katić, K., Li, R. & Zeiler, W. Thermophysiological models and their applications: A review. *Building and Environment* **106**, 286–300 (2016).
52. Harvie, G. N. Thermal behaviour in architectural fabric structures. in *Fabric Structures in Architecture* 221–240 (Woodhead Publishing, 2015). doi:10.1016/B978-1-78242-233-4.00008-5.
53. Peoples, J. *et al.* A strategy of hierarchical particle sizes in nanoparticle composite for enhancing solar reflection. *International Journal of Heat and Mass Transfer* **131**, 487–494 (2019).